ISSN 0036-0244, Russian Journal of Physical Chemistry A, 2018, Vol. 92, No. 11, pp. 2215–2226. © Pleiades Publishing, Ltd., 2018.

STRUCTURE OF MATTER AND QUANTUM CHEMISTRY

Study of CD_5^+ Ions and Deuterated Variants ($CH_xD^+_{(5-x)}$): An Artefactual Rotation[1]

Majid Monajjemi[a,*]

[a] *Department of Chemical Engineering, Central Tehran Branch, Islamic Azad University, Tehran, Iran*

**e-mail: m_monajjemi@srbiau.ac.ir*

Received October 15, 2017

Abstract—Deuterated methane, CD_5^+, has unusual vibrational and rotational behavior because its three non-equivalent equilibrium structures have nearly identical energies and its five protons scramble freely. Although a few theoretical papers have been published on the quantum mechanics of these systems, a better understanding requires spectral and conformational analysis. Post Hartree-Fock, Møller-Plesset and DFT calculations with the correlation consistent polarized valence double and triple zeta basis sets have been accomplished for estimating the thermodynamic data and zero-point energies of $CH_xD^+_{(5-x)}$. The present results indicates the normal modes agree with qualitative of $CH_xD^+_{(5-x)}$ which modes 10 indicates CD_5^+ is highly fluxional and has a complex spectrum while the C–D bonds which are broken and reformed all the time. The spectrum of mode 12 is highly complex with red-and some blue shifts. In particular, modes 8 and 10 be attributed to the rapid coupling of the CD-stretching normal mode to motions more closely related to isomerization, i.e., bending or rocking. There has thus been a long debate whether CD_5^+ has a structure at all or not and is it real rotational motions or artefactual.

Keywords: symmetry breaking, CH_5^+ ions, rotational motions

DOI: 10.1134/S0036024418110286

1. INTRODUCTION

Deuterated methane (CD_5^+) as a carbocation with three-center two-electron bonding has been subject of various theoretical and experimental investigations since its first detection in 1952 [1–7]. It is an important key intermediate in hyper-coordinated carbon chemistry and super-acid studies [8, 9] and is highly relevant in fields as plasma chemistry [10–12]. For decades and even up to now, CH_5^+ has provided some challenges due to the correlated large-amplitude motion of its five protons around the carbon for theoreticians and as well as for experimentalists.

In 2004 Keiran [13] and coworkers has applied a quantum diffusion Monte-Carlo (QDMC) calculation for estimating the ground-state zero-point energy from an interpolated PES. They have shown that the zero-point energy (ZPE) as a function of the number by 150 points has converged to within ±0.5 kJ/mol [13]. And also the converged fully an-harmonic ZPE on the interpolated PES calculated 132.72 was significantly lower than the CCSD(T)/aug-cc-pVTZ or MP2/cc-pVTZ harmonic zero-point energy of the global minimum structure, C_s, which were found 134.75 and 136.7 kJ/mol by Bowman and co-workers respectively [5].

Based on the bimodal character of the H–H radial distribution function, it is obvious that the ground-state of CH_5^+ wave function does have global minimum energy configuration C_s character; however, there is considerable delocalization of the protons and the calculated rotational constants proposed by Bowman [6], shows a ground-state structure with symmetrical structure than the C_s configuration. CH_5^+ consist of three configurations [14] including static equilibrium structure of ground state and two transition states, that mainly determine the dynamics of CH_5^+, they areas (1) e-C_s (I) isomer consists of a three-center two-electron bond associating two hydrogens and a CH_3 tripod, while H_2 moiety is attached in an eclipsed orientation. (2) A staggered (s-C_s) saddle-point [15], obtained by thirty degree rotation of the H_2 moiety, is barely higher in energy [16] (0.1 kcal mol^{-1}) than the ground state and (3) the third stationary point is a saddle-point [14, 15] with C_{2v} symmetry that is about ≈0.8 kcal mol^{-1} above the e-C_s global minimum structure [16]. An approach as a one of the scenarios enables easy

[1] The article is published in the original.

exchange of the hydrogen sites which so-called "hydrogen scrambling" [14]. This phenomenon has occurred by isomerization transitions between different degenerate stats of e-C_s minima through the s-C_s transition and C_{2v} structure [14, 17].

It might be understood from the zero point energy on the basis of the harmonic values which differ by some 100 cm^{-1} related to the location of the D atoms. According to the calculations of McCoy et al. [3], the lowest energy of the C_s (I) configuration was obtained for an arrangement where the three deuterons are placed in the tripod. Schreiner et al. calculated the harmonic zero-point energies of three species fore-C_s (I), s-C_s (II), and C_{2v} structures with amounts of 136.8, 136.4, and 132.0 kJ/mol, respectively and scaled their harmonic frequencies by 0.95 for estimating anharmonic effects [14]. Although those values are the best data comparison with the infrared spectra of CH_5^+ analysis, Keiran exhibited a reasonable amount of harmonic zero-point energy at 0.985 point on the CCSD (T)/aug'-cc-pVTZ interpolated PES [13]. Although based all five hydrogen atoms possess identical C–H and H–H radial distribution functions within the nuclear vibrational wave function, there is substantial proton scrambling, even at 0 K and this is an uncertain result of Keiran investigation.

Obviously, methane is a quasi-rigid molecule with a well-described molecular structure; however, for its protonation a deep discussion about its electronic structures is needed. This can be related to its abnormal flat potential energy which provides complicated. Large-magnitude motion for taking place which is a reason of fluxionality insists even at a very low temperature ($\neq$0 K) due to the QMF or quantum-mechanical fluctuation treatment of the highly correlated from the five protons scrambling motion [17].

In 2010 Ivanov [18] and coworkers through of deuterated variants of CH_5^+, exhibited that, in stark contrast to the traditional approach, the isotopologue spectra of $CH_xD_{(5-x)}^+$ (x = 0, 1, ..., 5), recorded in an ion trap using the Laser-Induced-Reactions [17] technique [18], bear almost no resemblance to one another [19, 20]. Through a SCF simulation [21] represent all six vastly [21] different IR spectra and allow for assigning their aspects. Analysis exactly confirms that the spectra observed for x = 1, 2, 3 H and D site occupations are confused but in the x = 4 a breaking of the combinatorial symmetry occurs for those atoms due to QMF within the fluxional molecular frame. There have been a few polemical discussions about the experiments which indicate that deuteron transfer from CD_4^+ to CH_4^+ can create stable isotopomers [22]. It is notable that the CD_4^+ and CH_4^+ have been generated by electron bombardment of methane at a very low pressure for avoiding reactions to CH_5^+, consequently the reaction of $CD_4^+ + CH_4^+ \rightarrow CH_xD_{(5-x)}^+$ might be happened [12].

Via an important procedure, D–H exchange reactions direct to isotope enrichment at low temperatures [5]. In 2004, Brown [6] via QDMC has reported the zero point energies for CD_5^+ and CH_5^+ as 8080 and 10975 cm^{-1}, respectively [6]. Due to C_s (I) structure described above, the $CD_3H_2^+$ isotopomer is of specific interest.

Although through hydrogen scrambling approach some of the complexity has been cleared for the quantum ground state of H_5^+ structure, in contrast of quotation in the citation [17, 18], hydrogen scrambling' is not the root of all the known intricacies [17, 18]. In particular, it has been discussed in this study that CH_5^+ undergoes hydrogen scrambling even in the quantum ground state and that the resulting correlated pseudo-rotational dynamics is done by symmetry braking consisting of several small barriers for variants $CH_xD_{(5-x)}^+$.

2. THEORETICAL BACKGROUND

Electron densities have been described as

$$\rho(r) = \eta_i |\varphi_i(r)|^2 = \sum_i \eta_i \left| \sum_l C_{l,i}\chi_i(r) \right|^2 \quad (1)$$

[23–25] and η_i is occupation number of orbitals (i), In addition φ_i are orbitals wave function, $\chi_i(r)$ are basis functions and $C_{l,i}$ are coefficient matrixes, the elements of ith row jth column correspond to the expansion coefficients of orbitals j respect to basis-set functions i. Electron densities can be explicitly written as e/Bohr [3].

$$\nabla\rho(r) = \left[\left(\frac{\partial\rho(r)}{\partial(x)} \right)^2 + \left(\frac{\partial\rho(r)}{\partial(y)} \right)^2 + \left(\frac{\partial\rho(r)}{\partial(z)} \right)^2 \right]^{\frac{1}{2}}, \quad (2)$$

$$\nabla^2\rho(r) = \frac{\partial^2\rho(r)}{\partial x^2} + \frac{\partial^2\rho(r)}{\partial y^2} + \frac{\partial^2\rho(r)}{\partial z^2} \quad (3)$$

[23–25]. The (–) and (+) values of these functions correspond to the electron densities are locally concentrated and locally depleted respectively. The chemical reactivity, chemical bond type, and electron localization has been built by Bader [26]. We have calculated densities of hydrogens and deuterium in deuterated variants of $CH_xD_{(5-x)}^+$ via the relationship between $\nabla^2\rho$ and valence shell electron pair repulsion (VSEPR) model [26].

Hamiltonian kinetic energies or $K(r)$ cannot be defined individually, since the expected value of

kinetic energy operator [25] $\left\langle \varphi \left| -\left(\frac{1}{2}\right)\nabla^2 \right| \varphi \right\rangle$ can be recovered by integrating kinetic energy densities from an alternative definition. One of popular used definition is

$$k(r) = -\frac{1}{2}\sum_i \eta_i \varphi_i^*(r)\nabla^2\varphi_i(r) \tag{4}$$

[23–25]. Relative to $K(r)$, the local definition given below guarantee positivizes everywhere; hence the physical meaning are clearer and are more generally used. The Lagrangian kinetic energies densities, $G(r)$ are also known as positive definition as:

$$G(r) = \frac{1}{2}\sum_i \eta_i |\nabla(\varphi_i)|^2 = \frac{1}{2}\sum_i \eta_i \left\{\left[\left(\frac{\partial\varphi_i(r)}{\partial(x)}\right)^2 + \left(\frac{\partial\varphi_i(r)}{\partial(y)}\right)^2 + \left(\frac{\partial\varphi_i(r)}{\partial(z)}\right)^2\right]\right\}. \tag{5}$$

$G(r)$ and $K(r)$ are directly related by Laplacian of electron densities

$$\frac{1}{4}\nabla^2\rho(r) = G(r) - K(r). \tag{6}$$

By kinetic energy definition via kinetic Monte-Carlo simulations the ground-state zero-point energy from an interpolated PES for estimating the ground-state zero-point energy can be calculated. It has been exhibited that the zero-point energy (ZPE) as a function of the number of distinct data by 150 points has converged to within ±0.5 kJ/mol [13]. According to transition state theory, the frequency with which hydrogen move to the H–H radial distribution function is expressed as:

$$\Gamma = \vartheta^* \exp\left(-\frac{\Delta E_h}{K_B T}\right), \tag{7}$$

where ΔE_h is the difference between the energy at an activated state and the initial equilibrium state, and ϑ^* is an effective vibrational frequency. In this work harmonic approximation of molecular vibrations, isotopes effects on uncoupled vibration is attained through rescaling of the frequency using the reduced masses ratio $\omega_D = \omega_H\sqrt{\frac{\mu_H}{\mu_D}}$ from the respective eigenfrequency $\omega_X = \omega_H\sqrt{\frac{K_X}{\mu_X}}$, supposing that the Born–Oppenheimer approximation holds $K_D = K_H$.

Edgecombe and Beck exhibited spin conditional pair probability has direct correlation with the Fermi hole as a novel electron localization function (ELF) [27].

$$\mathrm{ELF}(r) = \frac{1}{1 + [D(r)/D_{0(r)}]^2}, \tag{8}$$

where

$$D(r) = \frac{1}{2}\sum_i \eta_i |\nabla\varphi_i|^2 - \frac{1}{8}\left[\frac{|\nabla\rho_\alpha|^2}{\rho_\alpha(r)} + \frac{|\nabla\rho_\beta|^2}{\beta(r)}\right] \tag{9}$$

since

$$\rho_\alpha(r) = \rho_\beta(r) = \frac{1}{2}\rho, \tag{10}$$

D and D_0 terms can be simplified as

$$D(r) = \frac{1}{2}\sum_i \eta_i |\nabla\varphi_i|^2 - \frac{1}{8}\left[\frac{|\nabla\rho|^2}{\rho(r)}\right], \tag{11}$$

$$D_{0(r)} = \frac{3}{10}(3\pi^2)^{\frac{2}{3}}\rho(r)^{\frac{5}{3}}. \tag{12}$$

And also for a close-shell system it can be rewrite the Eq. (9) as:

$$D_{0(r)} = \frac{3}{10}(6\pi^2)^{\frac{2}{3}}\left[\rho_\alpha(r)^{\frac{5}{3}} + \rho_\beta(r)^{\frac{5}{3}}\right]. \tag{13}$$

Savin et al. have reinterpreted [28] ELF in the view of kinetic energy, which makes ELF also useful for Kohn-Sham wave-function in density functional theory. It has been indicated by Tsirelson and Stash that $D(r)$ reveals [29] the excess kinetic energy density caused by Pauli repulsion, while $D_0(r)$ can be considered as Thomas-Fermi kinetic energy densities.

Localized orbital locator (LOL) is defined and formulized by Schmider [30] and Becke as another novel function for locating high localization regions likewise ELF.

$$\mathrm{LOL}(r) = \frac{\tau(r)}{1 + \tau(r)} \tag{14}$$

and

$$r = \frac{D_0(r)}{\frac{1}{2}\sum_i \eta_i |\nabla\varphi_i|^2}, \tag{15}$$

$D_0(r)$ for spin-polarized system and close-shell system are defined in the same way as in ELF. In this study the ELF and LOL parameters of hydrogens and deuterium in deuterated variants of $CH_xD^+_{(5-x)}$ have been calculated for exhibiting the situation and position of five protons scrambling and their mechanism in real or artefactual rotational motions.

Local information entropies are the quantification of information which firstly was proposed by Shannonin his study about information transmission in noise channel mechanism. Nowadays their applications have been extremely widened to other areas, especially in theoretical chemistry. Many years ago Aslangul and coworkers attempted to decompose diatomic and triatomic molecules into reciprocal monopolized spaces through minimization of information entropies [31].

Parr et al. has discussed the relationship among information entropies and atomic partition and molecular similarities [32] and it has been exhibited the formula of Shannon's information entropies for normalized and continuous probability function is

$$S = -\int P(x)\ln P(x)dx, \quad (16)$$

while for the chemical systems, if $P(x)$ is replaced by $\frac{\rho(r)}{N}$, then the integrand may be called local information entropies of electrons [33]. Through the rearranging the formula it can be shown the

$$S(r) = -\frac{\rho(r)}{N}\ln\frac{\rho(r)}{N}, \quad (17)$$

where N is the total number of electrons in the chemical systems.

The electrostatic potentials (ESP) measure the electrostatic interaction among the unit point charges placed at r and the systems. A positive (negative) value implies that current position is dominated by nuclear (electronic) charges.

ESP has been widely used for prediction of statistical analysis, which Murray and coworkers found a set of function called GIPF [34] which connects ESP in molecular systems and macroscopic properties.

COMPUTATIONAL METHODS

Calculations were performed using Gaussian and GAMESS-US packages [35]. There is various situations of hydrogen and deuterium position interactions in the $CH_xD^+_{(5-x)}$ systems. The first PES and dipole moment using extensive direct-dynamics of the potential and gradient have been calculated at the CASSCF level of theory with cc-pVDZ and cc-pVTZ basis sets [36].

In this study full dimensional, ab-initio based potential energy surface and ab-initio electronic energies gradients are obtained through calculations using post HF, Møller-Plesset, and DFT theories with the correlation consistent polarized valence double and triple zeta basis sets.

Through redundant internal coordinates, several PESs in few inter-nuclear distances have been fit to these data. The potential energies and gradient data for each atoms of $CH_xD^+_{(5-x)}$ generated analytical multinomial expression, using Multiwfn analyzing software [23–25] as variables the complete set of inverse internuclear distances.

In this work, we have also focused on getting the optimized results from advanced DFT methods including the m06 and m06-L. The m062x, m06-L, and m06-HF are a novel Meta hybrid DFT functional with a good correspondence [37] and are useful for calculating the energies [38] of the distance between atoms in $CH_xD^+_{(5-x)}$. M06 and m06-L (DFT) functional is based on an iterative solution of the Kohn-Sham equation [39] in a plane-wave set with the projector-augmented wave pseudo-potentials. The Perdew-Burke-Ernzerhof [40] (PBE) exchange-correlation (XC) functional of the generalized gradient approximation (GGA) is adopted. Based our previous works [41–53] concerning the approaches of ELF, LOL, and density quantum energies, we strive to discuss a useful method for understanding more about $CH_xD^+_{(5-x)}$ treatments.

RESULTS AND DISCUSSION

The calculations are done for the optimization and zero-point energy determination of $CH_xD^+_{(5-x)}$ as well as for those compounds with reaction as follows: $CH_5^+ \rightarrow CH_3^+ + H_2$, $CHD_4^+ \rightarrow CD_3^+ + HD$, $CH_2D_3^+ \rightarrow CD_3^+ + H_2$, $CH_3D_2^+ \rightarrow CH_3^+ + H_2$, $CH_4D^+ \rightarrow CH_2D^+ + HD$, and $CD_5^+ \rightarrow CD_3^+ + D_2$. The fitted potential energy surface is tested by comparing it against additional electronic energy calculations and by comparing normal mode frequencies at the three lowest-lying stationary points obtained from the fitting against ab initio ones. Rotational constants along the C–X and H–X bond lengths and the tunneling coordinates via ELF, LOL, energy densities, Local information entropy, geometry optimization of variant $CH_xD^+_{(5-x)}$ (X = 0–5) and related normal modes have been calculated and are presented in Tables 1–8 and Figs. 1–9. In addition they have compared with the corresponding harmonic oscillator and standard classical molecular dynamics data. The delocalization of the wave function is analyzed through the Multiwfn software comparison of the CX_5^+ (X = H and D) distributions with those obtained when all of the hydrogen atoms are replaced by deuterium. The data of density energies, charges from ESP, electrostatic potential, ionization energy, ellipticity of electron densities, and Eta index for carbon, deuterium and hydrogens are listed in Tables 1–4.

ELF has been calculated via the Eq. (8) and as well as LOL has been done through Eqs. (14), (15). The variant densities for open and closed-shell systems have been estimated via Eqs. (9)–(13). The spin density from the difference between alpha and beta densities can be calculated through the expression of $\rho^s(r) = \rho^\alpha(r) - \rho^\beta(r)$, then the spin polarization parameter function returned instead of spin density $\xi(r) = \frac{\rho^\alpha(r) - \rho^\beta(r)}{\rho^\alpha(r) + \rho^\beta(r)}$. If electrons are completely localized, then they can be distinguished from those outside. Bader [26] found that the areas which have large electron localization might have large magnitudes of

Table 1. Energy densities, ELF, LOL, and local information for CD_5^+ via ccsd(T)/AUG-cc-pvdz

Atoms	D–C Bond length	Electron density	ESP (10^2)	Lagrangian kinetic [$G(r)$]	Hamiltonian kinetic [$K(r)$]	Potential energy Density [$U(r)$]	Electron localization function (ELF)	Local information entropy	Ellipticity of electron density	Eta index	Localized orbital locator (LOL)
C(1)	—	0.120	–0.166	0.531	0.166	–0.166	0.99	–0.300	0.000	–1.00	0.99
D(2)	1.09	0.349	–0.480	0.262	0.296	–0.299	0.99	0.117	0.001	–1.10	0.949
D(3)	1.09	0.348	–0.480	0.261	0.296	–0.298	0.99	0.117	0.001	–1.10	0.949
D(5)	1.11	0.330	–0.477	0.252	0.282	–0.285	0.99	0.113	0.002	–1.10	0.947
D(4)	1.20	0.297	–0.464	0.256	0.256	–0.259	0.99	0.104	0.026	–1.09	0.936
D(6)	1.20	0.287	–0.466	0.279	0.248	–0.251	0.99	0.102	0.035	–1.09	0.928

Table 2. Energy densities, ELF, LOL, and local information for CH_5^+ with CASSCF(8, 9)/cc-pvdz, quantum calculations

Atoms	C–H bond length	Electron density	Lagrangian kinetic [$G(r)$]	Hamiltonian kinetic [$K(r)$]	Potential energy Density [$U(r)$]	Electron localization function (ELF)	Local information entropy	Ellipticity of electron density	Eta index	Localized orbital locator (LOL)
H(2)	1.10	0.346	0.242	0.293	–0.295	0.99	0.116	0.001	–1.10	0.953
H(3)	1.10	0.346	0.242	0.293	–0.295	0.99	0.116	0.001	–1.10	0.953
H(5)	1.12	0.335	0.235	0.288	–0.290	0.99	0.113	0.001	–1.10	0.952
H(4)	1.24	0.300	0.238	0.260	–0.263	0.99	0.105	0.028	–1.09	0.942
H(6)	1.24	0.292	0.255	0.253	–0.255	0.99	0.103	0.035	–1.09	0.935

Table 3. ESP, energy densities, and LOL information for H atoms in variants $CH_xD_{(5-x)}^+$

Hydrogen properties in $CH_xD_{(5-x)}^+$	ESP (10^2)	Lagrangian kinetic [$G(r)$]	Hamiltonian kinetic [$K(r)$]	Potential energy Density [$U(r)$]	Electron localization function (ELF)	Local information entropy	Ellipticity of electron density	Eta index	Localized orbital locator (LOL)
CHD_4^+ : X = H(6)	–0.466	0.279	0.248	–0.251	0.99	0.102	0.035	–1.09	0.93
$CH_2D_3^+$: X = H(6)	–0.466	0.280	0.249	–0.252	0.99	0.102	0.036	–1.09	0.93
$CH_2D_3^+$: X = H(4)	–0.464	0.256	0.256	–0.259	0.99	0.104	0.026	–1.09	0.94
$CH_3D_2^+$: X = H(4)	–0.464	0.256	0.256	–0.259	0.99	0.104	0.025	–1.09	0.94
$CH_3D_2^+$: X = H(5)	–0.477	0.252	0.282	–0.285	0.99	0.113	0.002	–1.10	0.95
CH_4D^+ : X = H(2)	–0.464	0.256	0.256	–0.259	0.99	0.104	0.025	–1.09	0.94
CH_4D^+ : X = H(3)	–0.477	0.252	0.282	–0.285	0.99	0.113	0.002	–1.10	0.95
CH_5^+ : X = H(4)	–0.459	0.238	0.260	–0.263	0.99	0.105	0.028	–1.09	0.942
CH_5^+ : X = H(6)	–0.460	0.255	0.253	–0.255	0.99	0.103	0.035	–1.09	0.935

Fermi hole integration. Although $D_0(r)$ from Eqs. (11)–(13) is introduced into ELF as a reference, the ELF reveals basically a relative localization (ELF is within the range of [0, 1]). A large ELF values means that electrons are extremely localized, which indicates that there are covalent bonds in the regions. Based on ELF variables (as it can be seen in the Tables 1–4), all X–C strength bonds are equal with strong covalent bonds. As a result, the mechanism disassociation of the $CH_xD_{(5-x)}^+$ to produce H_2 or D_2 seems bizarre but is true. Ivanov [18] and coworkers have discussed through assigning the spectra of the isotopologues with experimental and computed IR spectra of CH_5^+

Table 4. ESP, energy densities, and LOL information for C atoms for variants $CH_xD^+_{(5-x)}$

Carbon properties in $CH_xD^+_{(5-x)}$	ESP (10^2)	Lagrangian kinetic [$G(r)$]	Hamiltonian kinetic [$K(r)$]	Potential energy Density [$U(r)$]	Electron localization function (ELF)	Local information entropy	Ellipticity of electron density	Eta index	Localized orbital locator (LOL)
CH_5^+	−0.166	0.531	0.166	−0.166	0.99	−0.300	0.000	−1.00	0.99
CHD_4^+	−0.166	0.531	0.166	−0.166	0.99	−0.300	0.000	−1.00	0.99
$CH_2D_3^+$	−0.166	0.531	0.166	−0.166	0.99	−0.300	0.000	−1.00	0.99
$CH_3D_2^+$	−0.166	0.531	0.166	−0.166	0.99	−0.300	0.000	−1.00	0.99
CH_4D^+	−0.166	0.531	0.166	−0.166	0.99	−0.300	0.000	−1.00	0.99

Table 5. Rotational temperatures, rotational constants, zero-point vibrational and E (thermal) for variants $CH_xD^+_{(5-x)}$

$CH_xD^+_{(5-x)}$	Molecular mass, amu	Rotational temperatures				Rotational constants (GHZ)			Zero-point vibrational energy (kcal/mol)	E (thermal) (kcal/mol)
		x	y	z	total					
CD_5^+	22.070	3.135	2.749	2.607	4.92	65.327	57.293	54.339	23.643	25.997
CHD_4^+	21.064	3.345	3.013	3.010	5.42	69.699	62.781	62.737	25.244	27.538
$CH_2D_3^+$	20.057	3.886	3.625	3.147	6.18	80.982	75.540	65.581	27.063	29.318
$CH_3D_2^+$	19.051	4.496	4.151	3.562	7.09	93.693	86.494	74.237	28.620	30.825
CH_4D^+	18.045	5.480	4.554	4.227	8.29	114.199	94.906	88.081	30.528	32.705
CH_5^+	17.039	6.258	4.818	4.562	9.11	130.40	100.392	95.05	31.744	33.811

Table 6. Zero-point and sum of electronic energies, C_v, and entropy for variants $CH_xD^+_{(5-x)}$

$CH_xD^+_{(5-x)}$	Sum of electronic and zero-point energies	Sum of electronic and thermal energies	Sum of electronic and thermal enthalpies)	Sum of electronic and thermal free energies	C_v, cal/(mol K)	S, cal/(mol K)
CD_5^+	−40.564275	−40.560524	−40.559579	−40.586386	10.662	56.419
CHD_4^+	−40.561723	−40.558069	−40.557125	−40.583540	10.229	55.596
$CH_2D_3^+$	−40.558824	−40.555232	−40.554288	−40.580354	9.822	54.860
$CH_3D_2^+$	−40.556343	−40.552831	−40.551886	−40.577516	9.548	53.941
CH_4D^+	−40.553303	−40.549834	−40.548890	−40.574168	9.211	53.201
CH_5^+	−40.544916	−40.541623	−40.540679	−40.565387	8.914	52.00

and all its H/D isotopologues (including mass-rescaled CD_5^+ and CH_5^+) with the simulated spectra to a particular mode (except for bends). Based on full decomposition into isotopomer contributions, they exhibited subsequent spectral disentangling proton occupation probabilities in the moiety where upper/lower bars indicate the quantum/classical distributions. It has been believed that within classical mechanics, the five different sites in the CX_5^+ are expected to be populated by H or D for all category of $CH_xD^+_{(5-x)}$.

Based on our results, it is supposed that only two bonds of C–X in a part of molecules exhibit properly quantum effects on the nuclei (as quantum particles through the high rotation) while remain parts of the molecules have classical particle behavior (lower rota-

Table 7. Normal modes vibrational temperatures for variants $CH_xD^+_{(5-x)}$

Normal modes vibrational temperatures	(1)	(2)	(3)	(4)	(5)	(6)	(7)	(8)	(9)	(10)	(11)	(12)
CD_5^+	258.97	884.05	1380.97	1382.59	1491.20	1497.38	1630.14	2458.32	2839.45	3158.17	3335.71	3478.36
CHD_4^+	288.91	999.87	1386.46	1455.70	1503.26	1619.40	1769.47	2718.52	3124.65	3337.03	3479.37	3724.56
$CH_2D_3^+$	303.56	1008.54	1503.01	1614.52	1641.15	1739.45	1875.54	2773.81	3211.15	3479.43	3724.63	4363.27
$CH_3D_2^+$	361.07	1011.69	1511.40	1642.40	1801.46	1822.70	2119.69	3203.36	3479.14	3479.82	3989.86	4382.13
CH_4D^+	361.92	1084.42	1609.64	1788.13	1945.17	1954.97	2225.82	3319.92	3479.32	3982.16	4374.54	4598.61
CH_5^+	586.38	1034.50	1679.75	1806.30	1990.12	2073.55	2104.00	2755.21	4229.01	4423.13	4583.55	4683.66

tion) which is so-called artefactual rotational motion. ELF has been widely used for wide variety of systems, such these kind of small molecules for revealing the atomic shell structure and the classification of chemical bonding to verify charge-shift bonds. This approach became stronger via LOL data which has similar expression compared to ELF. Jacobsen pointed out that LOL conveys more decisive and clearer picture than ELF; obviously LOL can be interpreted in kinetic energy in the same way as for ELF; however LOL can also be interpreted in point view of localized orbital. Small (large) LOL values usually appear in the boundary (inner) area of localized orbitals because the gradient of the orbital wave-function is large (small) in this area. The value range of LOL is identical to ELF, namely [0, 1]. As it can be seen in the Tables 1 and 2 the values of LOL are different for two levels of classical occupations and quantum populations.

Normal mode analyzing has been exhibited protons are prefer to accumulate in the X_2 moiety for all mixed isotopologues whereas deuterons prefer to be in the CX_3 tripod based on quantum approaches (Tables 5–7 and Figs. 7–9). Average local ionizations for separated fragments are shown in Fig. 6 that indicates the energy separation is a function of HD situation, which are equal for $CH_4D^+ \rightarrow CH_2D^+ + HD$ and $CHD_4^+ \rightarrow CD_3^+ + HD$ and different for $CH_5^+ \rightarrow CH_3^+ + H_2$ and $CD_5^+ \rightarrow CD_3^+ + D_2$. The C(1)–H(6) stretching band as a lowest-frequency has been associated with the relative motion of the H_2 moiety with respect to the methyl tripod in Protonated methane which indicates that CH_5^+ is actually composed of those two subunits, CX_3 and X_2 in the hydrogen scrambling. So, the results indicate that H atoms freely exchange by passaging over the isomerization barriers energy between C_{2v} and C_s levels of energy. The neutralization of protonated methane

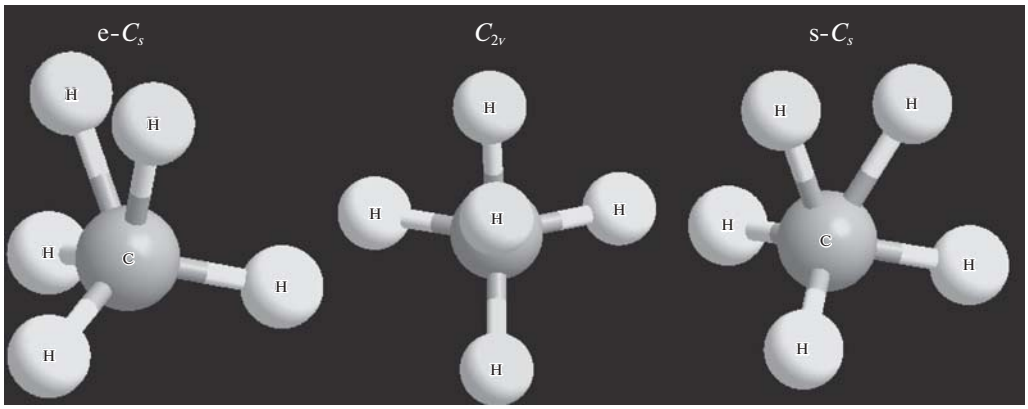

Fig. 1. Eclipsed (e-C_s for global minima) structures with CH_3 tripod (white and gray), staggered saddle point (s-C_s for the transition state for H_2 rotation) and H_2 moiety (yellow); saddle point structure (C_{2v} for H_2–CH_3 proton exchange) with three coplanar hydrogen atoms (yellow).

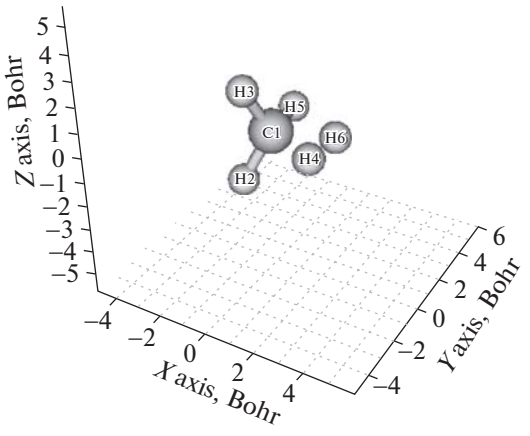

Fig. 2. The H(6) and H(4) hydrogens prefer to be out of the CX_3 tripod based on quantum approaches.

by opposite rearranging with free electrons is one of importance approaches for this study.

Energy level diagram (Fig. 6 and Table 5) shows the two energetically accessible dissociation limits of CH_5^+ which is formed with C_s on the neutral surface. The three-body dissociation limit is nearly resonant with the 3*s* Rydberg state. The results of ellipticity of electron density from Tables 1–4 described using the correct "fluxional" phase-spaces sampling of CH_5^+ which are vertical, resonant, and non-resonant in good corresponding with the experimental data.

In Fig. 6 the shoulder near 1.714 Bohr corresponds to D_2 moiety, whereas the peak at 2.114 Bohr corresponds to H–D groups. Moreover, the shoulder near 2.5 Bohr corresponds to the H_2 moiety. It is clear that most of the energy goes into internal excitation (vibrational and rotational) of the $CH_3^+ + H_2$. This channel exhibits a bimodal distribution that the explanation for this shoulder comes from consideration of the HH, HD, and DD bond lengths distribution in the parent $CH_xD_{(5-x)}^+$ and the portion of that distribution correlates with $CX_3 + X_2$ products more significantly which are shown in Figs. 4–6.

Ivanov et al. [18] have shown that classical ab initio molecular dynamics indeed reproduces closely the binomial distributions expected for those site occupations while the full quantum simulations reveal the quantum populations strongly deviating from classical (binomial) occupations. Here, there is a point; is there any real or artefactual rotational motion in quantum approaches? In other words, there is a symmetry breaking among classical towards quantum approaches only for X_2 as a part of molecule. On par-

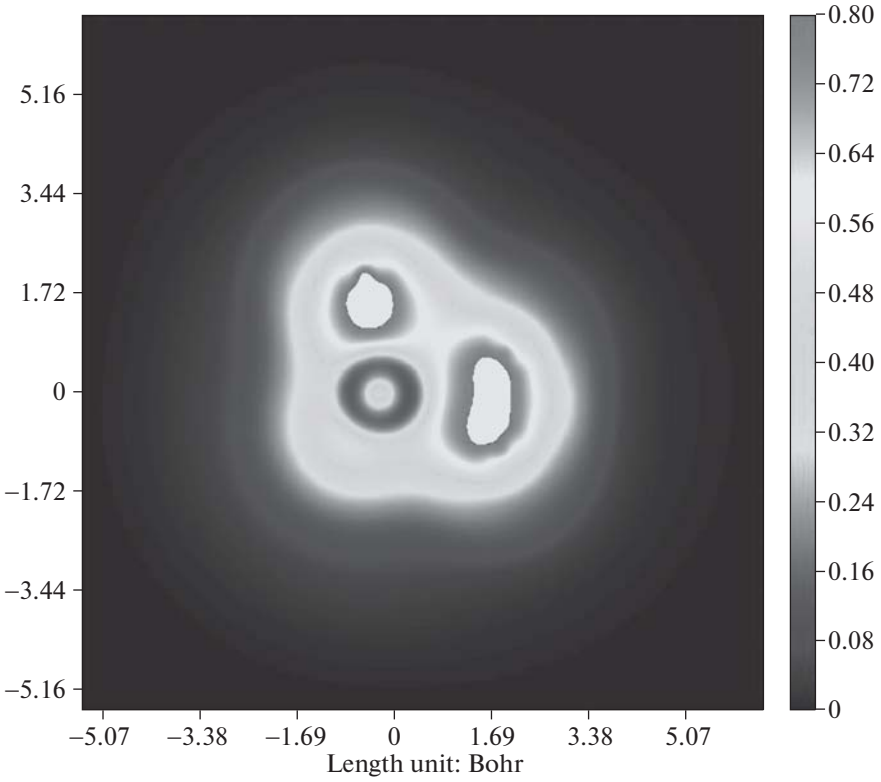

Fig. 3. LOL calculation and color-filled map of CH_5^+ through Casscf(8,9)/cc-pvdz calculation.

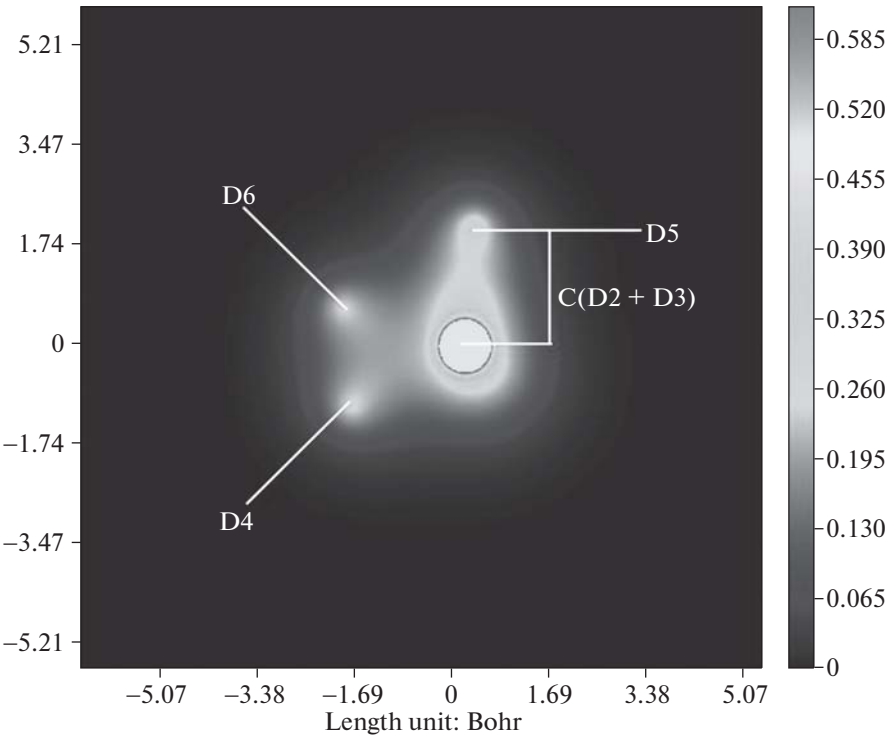

Fig. 4. Electron density color-field map for $CD_5^+ \rightarrow CD_3^+ + D_2$ separation.

tial D ↔ H substitutions, scrambling phenomenon appeared in different isotopic nuclei for populating all available sites, that is, those in the X_2 moiety. The local information entropy data in Tables 1–4 and entropy in Table 6 indicate that $CH_xD^+_{(5-x)}$ is binomial distributions but for two parts inside the molecule. Considering the differences in zero-point energies of D and H, it might be indicated that deuterons prefer to populate the CX_3 tripod in the mixed isotopologues CH_4D^+ and CHD_4^+, whereas protons conjecture in the X_2 moiety are compared to the purely combinatory probabilities.

Quantum-mechanical fluctuations due to Boltzmann statistics cause systematic deviations of the H and D sites from the underlying combinatorial symmetries, and thereby induce a breaking of that symmetry. The Localized orbital locator and electron localization function (Tables 1–4) have confirmed the approaches of quantum localization in this work. This effect is relevant at all for the vibrational normal modes and as it can be seen, these intricate nuclear quantum effects are certain ways for understanding the experimental spectra [54].

Distribution correlating with CH_3^+ and H_2 exhibits a larger contribution with the shorter one of H–H distance than the longer one. In addition, vibrational excited state of H–H with the larger hydrogen–hydrogen bond length indicates a greater contribution than the shorter one (in contrast D–D), while for H–D, it depends to isotopologues combinations.

Through the normal modes analysis, it can be seen that partial D ↔ H substitutions break the rotational symmetry.

CONCLUSIONS

The present results of the mode 8, 12, and 10 agree with qualitative of CH_5^+ which are highly fluxional and have a complex spectrum while the C–X bonds are broken and reformed all the time via quantum/classical distributions of two terms for X–X (X = H or D) and segment remain of the molecule. Therefore the simple model of balls and sticks does not apply. The spectrum of mode 12 is highly complex with huge red-shifts and some blue-shifts. In particular, they can be attributed to the rapid coupling of the original CH-stretching normal mode to motions more closely related to isomerization, i.e., bending or rocking. There has thus been a long debate whether CH_5^+ has a structure at all or not and it has real or artefactual rotational motions. It is supposed that only two bonds of C–X in a part of molecules obey quantum populations while remain parts of the molecules have a classical occupations which there is an artefactual rotational motion in $CH_xD^+_{(5-x)}$.

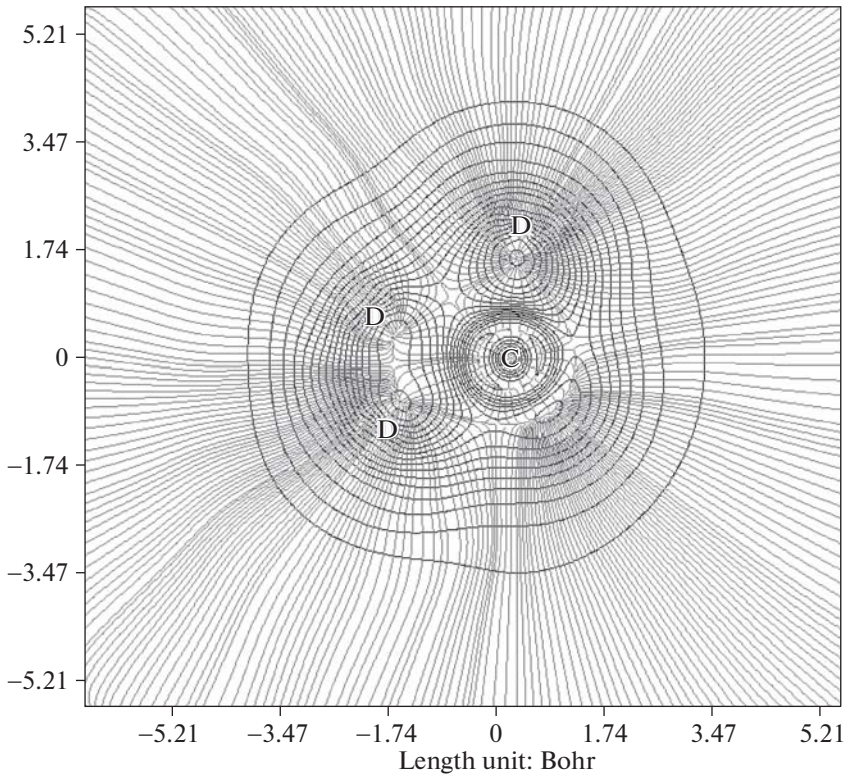

Fig. 5. LOL gradient lines map of CD_5^+ in a quantum rotation.

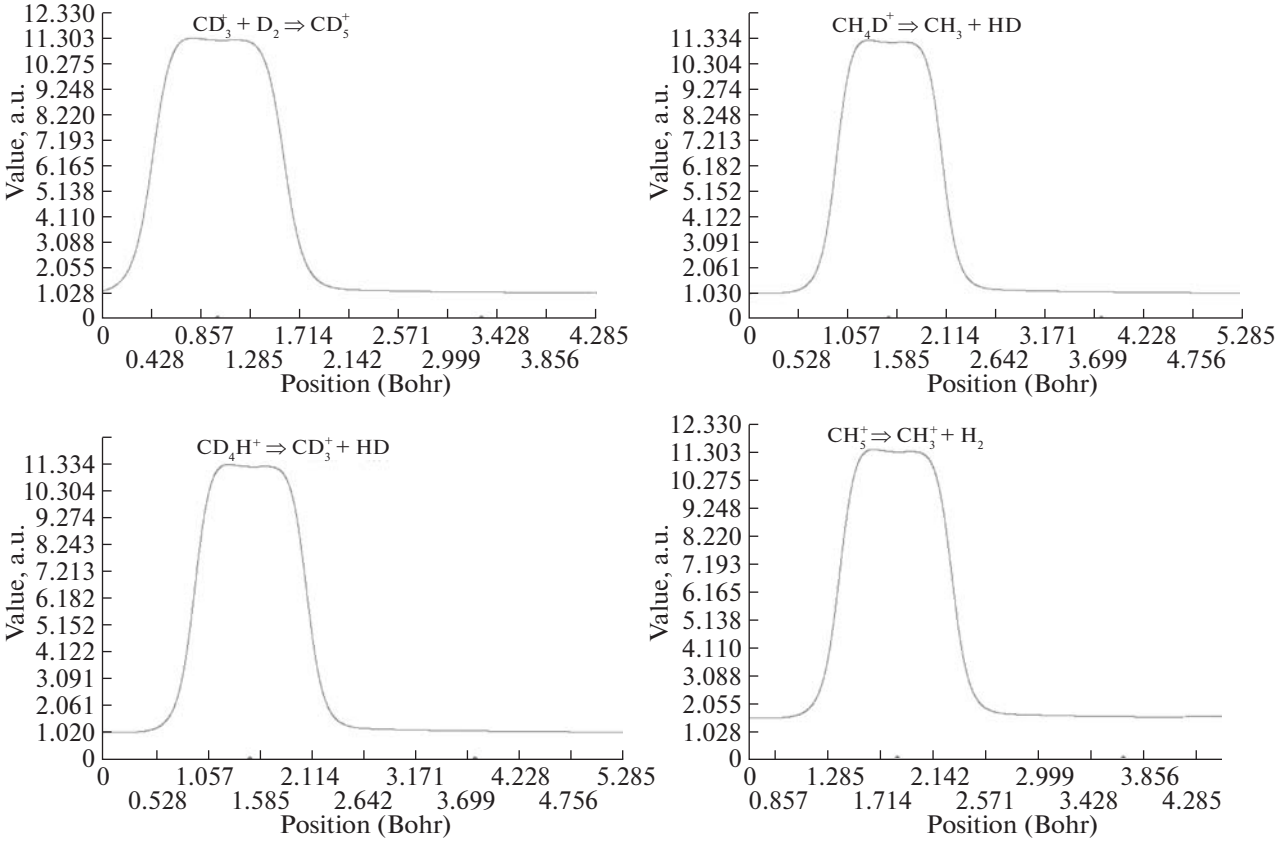

Fig. 6. Average local ionization energy for CH_5^+, CD_5^+, CH_4D^+, and CHD_4^+.

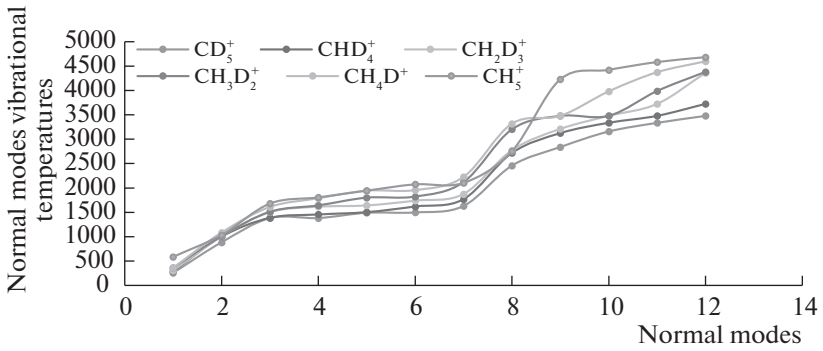

Fig. 7. Normal modes vibration temperature for variants $CH_xD^+_{(5-x)}$.

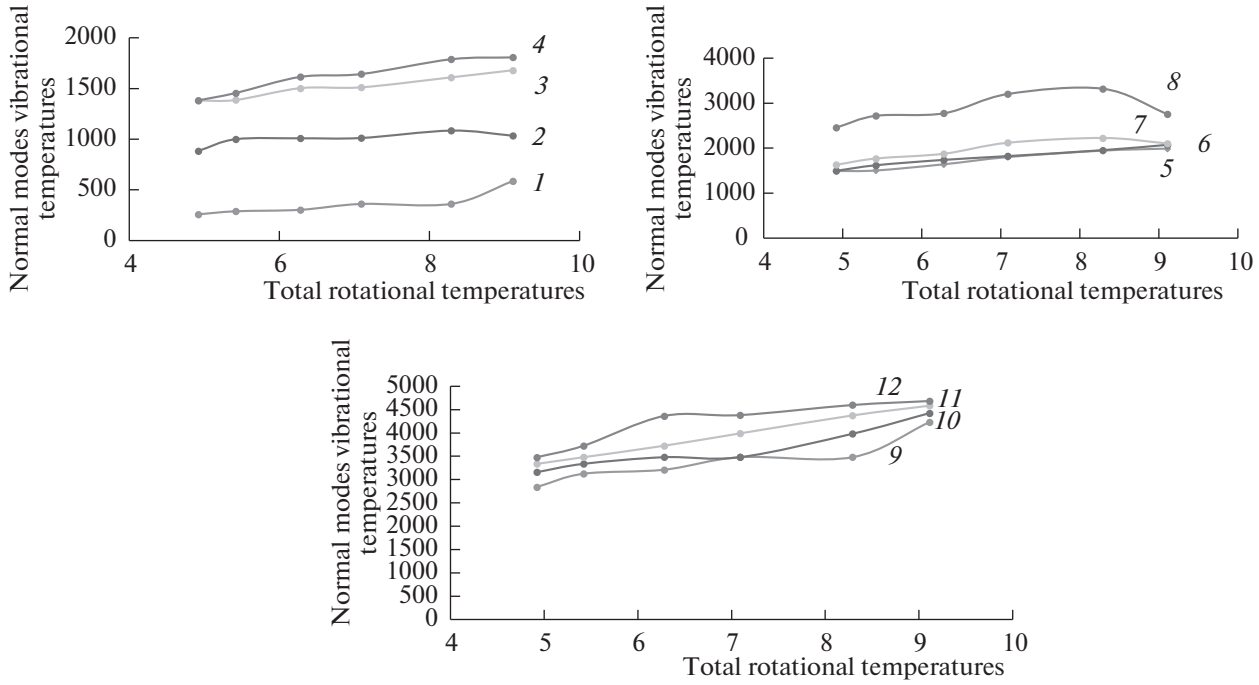

Fig. 8. Normal modes vibration temperature vs. rotational temperatures for variants $CH_xD^+_{(5-x)}$.

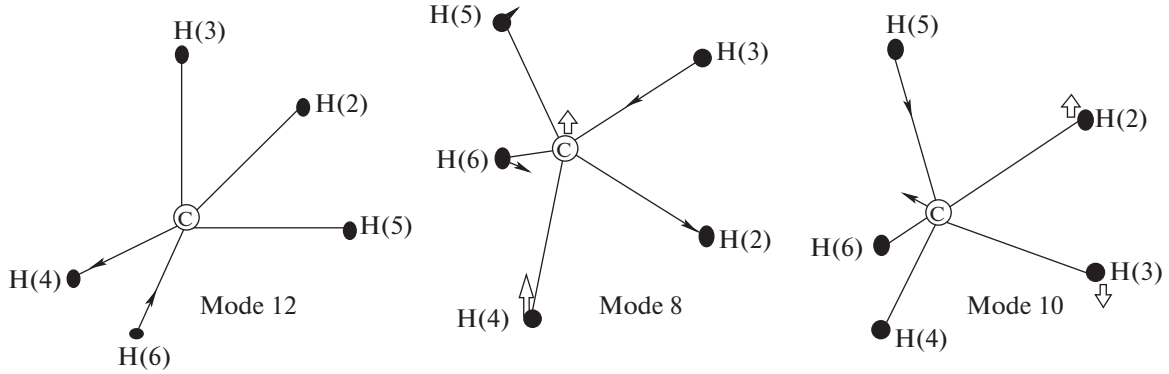

Fig. 9. Frequencies 8, 10, 12 modes of vibrations.

REFERENCES

1. D. Marx and M. Parrinello, Science (Washington, DC, U. S.) **284**, 59 (1999).
2. P. R. Schreiner, Angew. Chem. Int. Ed. **39**, 3239 (2000).
3. A. B. McCoy, B. J. Braams, A. Brown, Xinchuan Huang, Zhong Jin, and J. M. Bowman, J. Phys. Chem. A **108**, 4991 (2004).
4. A. L. Kaledin, S. D. Kunikeev, and H. S. Taylor, J. Phys. Chem. A **108**, 4995 (2004).
5. A. Brown, B. J. Braams, K. Christoffel, Z. Jin, and J. M. Bowman, J. Chem. Phys. **119**, 8790 (2003).
6. A. Brown, A. B. McCoy, B. J. Braams, Z. Jin, and J. M. Bowman, J. Chem. Phys. **121**, 4105 (2004).
7. G. A. Olah and G. Rasul, Acc. Chem. Res. **30**, 245 (1997).
8. G. A. Olah, G. K. S. Prakash, and J. Sommer, *Superacids* (Wiley, Chichester, 1985), Chaps. 3, 5.
9. G. A. Olah, G. K. S. Prakash, R. E. Williams, L. D. Field, and K. Wade, *Hypercarbon Chemistry* (Wiley, Chichester, 1987), Chaps. 1, 5, 7.
10. T. Oka, Philos. Trans. R. Soc. London, A **324**, 81 (1988).
11. E. Herbst, J. Phys. Chem. A **109**, 4017 (2005).
12. D. Gerlich, Phys. Chem. Chem. Phys. **7**, 1583 (2005).
13. K. C. Thompson, D. L. Crittenden, and M. J. T. Jordan, J. Am. Chem. Soc. **127**, 4954 (2005).
14. P. R. Schreiner, S.-J. Kim, H. F. Schaefer III, and P. V. R. Schleyer, J. Chem. Phys. **99**, 3716 (1993).
15. V. Dyczmons and W. Kutzelnigg, Theor. Chim. Acta (Berlin) **33**, 239 (1974).
16. H. Müller, W. Kutzelnigg, J. Noga, and W. Klopper, J. Chem. Phys. **106**, 1863 (1997).
17. D. Marx and M. Parrinello, Nature (Lodnon, U.K.) **375**, 216 (1995).
18. S. D. Ivanov, O. Asvany, A. Witt, E. Hugo, G. Mathias, B. Redlich, D. Marx, and S. Schlemmer, Nat. Chem. **2**, 298 (2010).
19. S. Schlemmer, E. Lescop, J. von Richthofen, D. Gerlich, and M. A. Smith, J. Chem. Phys. **117**, 2068 (2002).
20. S. Schlemmer and J. Asvany, J. Phys.: Conf. Ser. **4**, 134 (2005).
21. D. Marx and J. Hutter, *Ab initio Molecular Dynamics: Basic Theory and Advanced Methods* (Cambridge Univ. Press, 2009).
22. A. J. R. Heck, L. J. de Koning, and N. M. M. Nibbering, J. Am. Soc., Mass. Spectrom. **2**, 453 (1991).
23. T. Lu and F. Chen, Acta Chim. Sin. **69**, 2393 (2011).
24. T. Lu and F. Chen, J. Mol. Graph. Model. **38**, 314 (2012).
25. T. Lu and F. Chen, J. Comput. Chem. **33**, 580 (2012).
26. R. F. W. Bader, *Atoms in Molecule: A Quantum Theory* (Oxford Univ. Press, Oxford, 1990).
27. A. D. Becke and K. E. Edgecombe, J. Chem. Phys. **92**, 5397 (1990).
28. A. Savin et al., Angew. Chem. Int. Ed. Engl. **31**, 187 (1992).
29. V. Tsirelson and A. Stash, Chem. Phys. Lett. **351**, 142 (2002).
30. H. L. Schmider and A. D. Becke, J. Mol. Struct.: THEOCHEM **527**, 51 (2000).
31. C. Aslangul et al., Adv. Quantum Chem. **6**, 93 (1972).
32. R. G. Parr et al., J. Phys. Chem. A **109**, 3957 (2005).
33. S. Noorizadeh and E. Shakerzadeh, Phys. Chem. Chem. Phys. **12**, 4742 (2010).
34. J. S. Murray et al., J. Mol. Struct.: THEOCHEM **307**, 55 (1994).
35. M. W. Schmidt, K. K. Baldridge, J. A. Boatz, S. T. Elbert, M. S. Gordon, J. H. Jensen, S. Koseki, N. Matsunaga, K. A. Nguyen, et al., J. Comput. Chem. **14**, 1347 (2004). doi 10.1002/jcc.540141112
36. T. H. Dunning, Jr., J. Chem. Phys. **90**, 1007 (1989).
37. Yan Zhao and D. G. Truhlar, Theor. Chem. Account **120**, 215 (2008).
38. W. Kohn and L. J. Sham, Phys. Rev. A **140**, 1133 (1965).
39. J. P. Perdew and K. Burke, Ernzerhof, Phys. Rev. Lett. **77**, 3865 (1996).
40. D. L. Klein, R. Roth, A. K. L. Lim, A. P. Alivisatos, and P. L. McEuen, Nature (London, U.K.) **389**, 699 (1997).
41. M. Monajjemi and J. E. Boggs, J. Phys. Chem. A **117**, 1670 (2013). doi 10.1021/jp312073q
42. M. Monajjemi, V. S. Lee, M. Khaleghian, B. Honarparvar, and F. Mollaamin, J. Phys. Chem. C **114**, 15315 (2010). doi 10.1021/jp104274z
43. M. Monajjemi, J. Mol. Model. **20**, 2507 (2014). doi 10.1007/s00894-014-2507-y.
44. M. Monajjemi, Theor. Chem. Acc. **134**, 77 (2015). doi 10.1007/s00214-015-1668-9
45. M. Monajjemi, Struct. Chem. **23**, 551 (2012). doi 10.1007/s11224-011-9895-8
46. M. Monajjemi, Chem. Phys. **425**, 29 (2013). doi 10.1016/j.chemphys.2013.07.014
47. H. Jalilian and M. Monajjemi, Jpn. J. Appl. Phys. **54**, 085101 (2015). doi 10.7567/JJAP.54.085101
48. M. Monajjemi and M. Khaleghian, J. Clust. Sci. **22**, 673 (2011). doi 10.1007/s10876-011-0414-2
49. M. Monajjemi, M. Falahati, and F. Mollaamin, Ionics **19**, 155 (2013). doi 10.1007/s11581-012-0708-x
50. M. Monajjemi, Biophys. Chem. **207**, 114 (2015). doi 10.1016/j.bpc.2015.10.003
51. L. Mahdavian and M. Monajjemi, Microelectron. J. **41**, 142 (2010). doi 10.1016/j.mejo.2010.01.011
52. M. Monajjemi, J. Mol. Liq. **230**, 461 (2017). doi 10.1016/j.mejo.2010.01.011
53. M. Monajjemi, Macedon. J. Chem. Chem. Eng. **36**, 101 (2017). doi 10.20450/mjcce.2017.1134
54. E. Herbst, J. Phys. Chem. A **109**, 4017 (2005).